East European Journal of Physics. 3. 298-308 (2025)
DOI:10.26565/2312-4334-2025-3-27 ISSN 2312-4334

STRUCTURAL, ELECTRONIC AND ELASTIC PROPERTIES OF POTASSIUM IODIDE, UNDER PRESSURE: AN AB-INITIO ANALYSIS STUDY

Hamza Rekab-Djabri[a,b]*, S. Zaiou[c,d], Ahmed Azzouz-Rached[e], Ammar Benamrani[f], Salah Daoud[g], D. Belfennache[h], R. Yekhlef[h], Nabil Beloufa[i]

[a]*Laboratory of Micro and Nanophysics (LaMiN), National Polytechnic School Oran, ENPO-MA, BP 1523 El M'Naouer 31000, Oran, Algeria*
[b]*Faculty of Nature and Life Sciences and Earth Sciences AMO University, Bouira 10.000, Algeria*
[c]*Laboratory for Studies of Surfaces and Interfaces of Solid Materials (LESIMS), University Setif 1, 19000 Setif, Algeria*
[d]*Faculty of Natural Sciences and Life, Setif-1 University, 19000 Setif, Algeria*
[e]*Faculty of Sciences, Saad Dahleb University of Blida 1, Route de Soumaa, B. P. 270, Blida, Algeria*
[f]*Laboratory of Materials Physics, Radiation and Nanostructures (LPMRN), Faculty of Sciences and Technology, University of Mohamed El Bachir El Ibrahimi-BBA, 34000, Bordj Bou Arreridj, Algeria*
[g]*Laboratory of Materials and Electronic Systems, Faculty of Sciences and Technology, University Mohamed El Bachir El Ibrahimi of BBA, 34000 Bordj Bou Arreridj, Algeria*
[h]*Research Center in Industrial Technologies CRTI, P.O. Box 64, Cheraga, 16014 Algiers, Algeria*
[i]*Hydrometeorological Institut for Formation and Research IHFR, Oran, Algeria*
**Correspondence Author E-mail: belfennachedjamel@gmail.com*
Received May 14, 2025; revised July 16, 2025; accepted July 28, 2025

In this work, a recent version of the full potential linear muffin-tin orbitals (FP-LMTO) method was employed, using the local density approximation (LDA) within the framework of density functional theory (DFT). This approach was applied to study the structural, electronic and elastic behavior of the potassium iodide (KI) compound under pressure. The calculated structural parameters exhibit strong agreement with available theoretical and experimental data. The RS phase was identified as the most stable structure for KI material. The phase transition from NaCl-type (B1) to CsCl-type (B2) phase occurs at pressure of 1.633 GPa, which is quite consistent with the experimental values. Furthermore, the band structure of KI revealed a wide-band gap semiconductor behavior across all examined phases. The obtained bulk modulus values were relatively low, suggesting weak resistance to fracture. The elastic constants for KI in RS, CsCl, ZnS, HCP, and WZ structures were determined and found to meet Born's stability conditions. We esteem, there is no values available in the literature on the elastic constants for KI in CsCl, ZnS and WZ phases. All analyzed structures displayed ductile characteristics and ionic bonding features. Additionally, anisotropic properties were observed in all phases. The compound's stiffness was evaluated using Poisson's ratio and Cauchy's pressure. Results indicated that the CsCl phase is the most rigid among the studied configurations.
Keywords: *Potassium iodide (KI); FP-LMTO; Electronic properties; Elastic properties; Phase transition*
PACS: 73.50.-h, 73.50.Pz

1. INTRODUCTION

Alkali halides, such as potassium iodide (KI), are known as insulating salts composed of alkali metal cations and halide anions, with ions derived from group IA and VIIA elements in the periodic table. Under standard conditions, these materials typically crystallize in the Rocksalt (RS) structure [1]. Alkali iodides have played a crucial role in solid-state physics research since the 20th century [2-6], and continue to do so in more recent studies [7-9]. They have attracted considerable interest due to their unique features, such as crystal structure transitions under elevated pressures. Within the alkali halide family, potassium iodide (KI) has been specifically selected for this investigation. These compounds are widely recognized in the scientific community. KI, for instance, is frequently cited in nanoscience research, including studies involving single-walled carbon nanotubes [10,11].

Additionally, KI and similar materials are utilized in chemical processes and have notable medical applications, particularly in thyroid-related treatments. While KI has been examined both experimentally and theoretically in its RS phase across various studies, its other structural forms have received less attention. As an example, for the RS phase, the experimental lattice constant was reported as 7.094 Å [7], while in the CsCl structure it measured 7.342 Å [12]. The bulk modulus (B) for KI was experimentally found by Weir et al. [13] to be 11.6 GPa, whereas theoretical results from Cortona *et al.* [14] suggest a value of 13.8 GPa. A particularly interesting aspect of alkali halides is their capacity to undergo phase changes under low pressure. The pressure at which such structural phase transitions occur is referred to as the transition pressure (Pt).

According to experiments, at comparatively low pressures, a phase change from the RS structure (B1) to the CsCl structure (B2) takes place. For KI, transition pressure values were determined by Asaumi *et al.* [5] to be 1.9 GPa and Barsch *et al.* [17] to be 1.73 GPa. In the RS structure, the electrical characteristics of KI have been examined. Teegarden *et al.* [20] determined the energy band gap (Eg) values from absorption spectra graphs, and the values for KI

Cite as: H. Rekab-Djabri, S. Zaiou, A. Azzouz-Rached, A. Benamrani, S. Daoud, D. Belfennache, R. Yekhlef, N. Beloufa, East Eur. J. Phys. 3, 298 (2025), https://doi.org/10.26565/2312-4334-2025-3-27

in the RS structure were 6.1 eV and 6 eV. Hopfield *et al.* [21] conducted additional experimental work that yielded an energy band gap of 6.34eV for KI in the RS structure. The energy band gap for both KI in RS was also calculated. Using the full potential linearized muffin-tin orbital (FP-LMTO) method, the results showed that the KI was 5.984 eV [7], 4.26 eV [22], and 5.951 eV [23]. The first-principles linearized augmented-plane-wave band method yielded the same results. These energy band gap data show that the compound KI in the RS structure exhibits wide-band gap semiconducting properties. Numerous elastic constants and moduli, including the bulk and young moduli, can be used to depict the elastic properties of any compound. But for cubic structures, the most fundamental elastic constants are C_{11}, C_{12}, and C_{44}; for hexagonal structures, there are two more: C_{13} and C_{33}. Numerous theoretical and experimental approaches have been used to examine the elastic constants for KI. Using the ultrasonic pulse technique, Norwood and Briscoe determined the elastic constants for KI and discovered that C_{11}, C_{12}, and C_{44} have values of 27.1, 4.5, and 3.64 GPa, respectively [24]. Bridgman reported C_{11}, C_{12}, and C_{44} values of 33.2, 5.78, and 6.2 GPa [25]. The homogenous deformation method, on the other hand, served as the foundation for Sarkar and Sengupta's theoretical computation of the elastic constants, which yielded values of 31.7, 3.2, and 4.2 GPa for C_{11}, C_{12}, and C_{44}, respectively [19]. Lastly, Gahn *et al.* [26] determined the Young modulus to be 15.3 GPa.

This study attempts to increase our understanding of the structural, elastic, and electrical characteristics of the compound KI in the following structures: wurzite (WZ), hexagonal close packed (A3), zincblende (ZB), nickel arsenide (NiAs), rock salt (RS), and cesium chloride (CsCl).

2. COMPUTATIONAL DETAILS

Within the functional of density functional theory (DFT) [27-29], the FP-LMTO method, as implemented in the LMTART code [30], was used to accomplish the computations given in this work. We employed the local density approximation (LDA) for exchange correlation potential, as specified by *Benkrima et al.* [31-33], for the electron-electron interaction in the total energy calculations. Using spherical harmonics, the electron charge density and crystal potential inside muffin-tin (MT) spheres were increased up to lmax = 6. The parameters utilized in the current computations are listed in Table 1 and include the radius of the muffin-tin (RMT) spheres, the number of plane waves (NPLW) employed, and the kinetic energy required to guarantee convergence (Ecutoff) for each of the eight crystal structures that were examined.

Table 1. The plane wavenumber NPLW, energycut-off (in Ry) and the muffin-tin radius (RMT) (in a.u) used in calculation for binary KI.

Structure	NPLW	E_{cut}tot(Ry)	RMT(u.a)	
	KI	KI	K	I
NaCl(B1)	223	12.6	3.26	3.393
CsCl(B2)	215	11.1	3.496	3.496
ZnS(B3)	228	11	3.058	3.313
Wz(B4)	390	9.1	3.046	3.224
NiAs(B8-1)	136	21.7	3.236	3.368
HCP (A3)	136	21.7	3.807	3.807

In the cubic symmetry of the NaCl (B1), CsCl (B2), and ZnS (B3) structures shown in Fig. 1(a, b, and c), the unit cell volume is solely dependent on the lattice constant a.

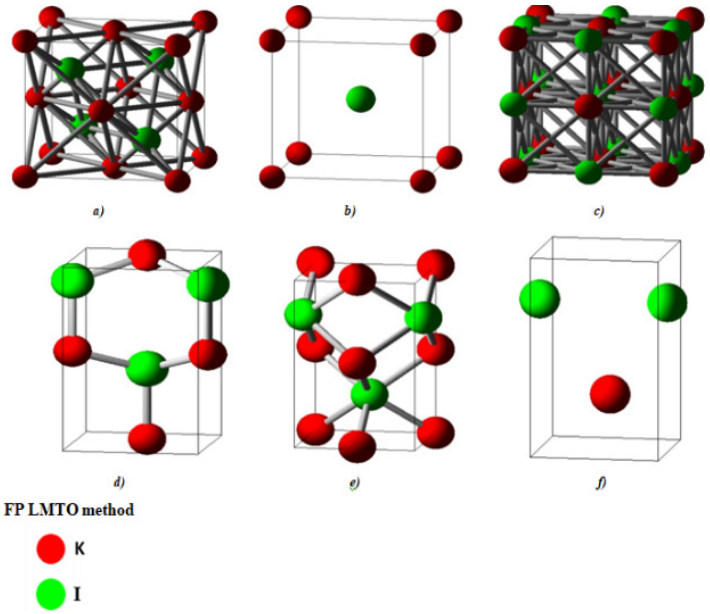

Figure 1. Crystal structure of KI in **a**-NaCl(B1), **b**-CsCl(B2), **c**-ZnS(B3), **d**- Wurtzite (B4), **e**-HCP(A3), and **h**-NiAs(B8_1)

The unit cell volume in other structures, such as wurtzite (B4), NiAs (B81), and HCP (A3), as shown in Fig. 1(d, e, and f), relies on several lattice constants (z, a, c/a ratio, and internal parameter u); hence, each of these structures needs to be optimized. Table 2 lists the locations of the potassium (K) and iodide (I) atoms in each of the KI compound's aforementioned structures.

These structures have the following space groups: B1: *Fm3m*, B2: *Pm3m*, B3: *F43m*, B4: *P63mc*, A3: *P63/mmc*, and B81: *P63/mmc.*

Table 2. Location of atoms for the six phases

	Potassiom (K)		Iodide (I)	
	1st atom	**2nd atom**	**1st atom**	**2nd atom**
NaCl(B1)	0.0 ;0.0 ;0.0		1/2; 1/2; 1/2	
CsCl(B2)	0.0 ;0.0 ;0.0		1/2; 1/2; 1/2	
ZnS(B3)	0.0 ;0.0 ;0.0		1/4; 1/4; 1/4	
Wz(B4)	0.0 ;0.0 ;0.0	1.2; -1/2√3; 1/2	0.0; 0.0; u	1.2; -1/2√3; (0.5+u)
NiAs(B8-1)	0.0 ;0.0 ;0.0	0.0; 0.0; 1/2	1.2; 1/√12; 1/4	1.2; -1/√12; 3/4
HCP (A3)	1.2; 1/2√3; 1/4		1.2; 1/2√3; 3/4	

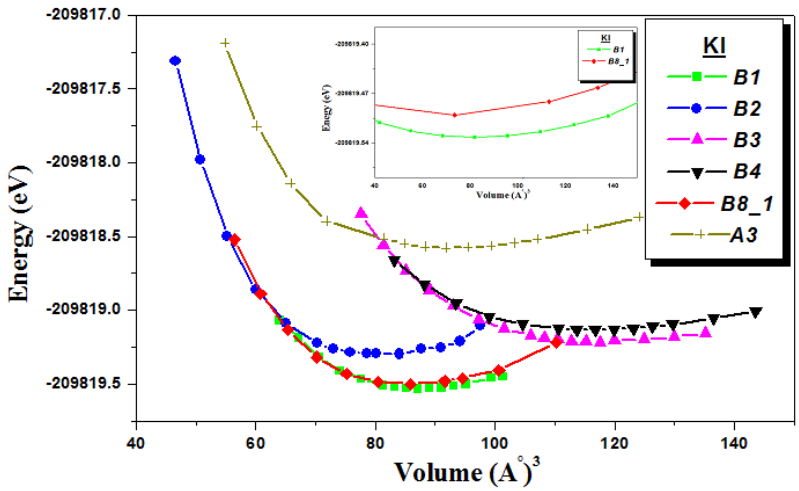

Figure 2. Total energy versus volume for six phases of KI in the LDA approximation

3. RESULTS AND DISCUSSION

3.1. Structural phase stability

We plotted the E(V) curves in this work to determine the structural properties of the semiconductor compound KI for each of the six structures considered: NaCl (B1), CsCl (B2), ZnS (B3), Wurtzite (B4), NiAs (B8_1) and HCP (A3). Using the Murnaghan equation of state (EOS), which can be written as follows [27], the equilibrium lattice constant a0, the bulk modulus B_0 and the pressure derivative of the bulk modulus B_0' were calculated by minimizing the total energy.

$$E(V) = E_0 + \frac{B0}{\acute{B}0(\acute{B}0-1)}\left[V\left(\frac{V_0}{V}\right)^{B0} - V_0\right] + \frac{B0}{\acute{B}0}(V - V_0), \quad (1)$$

with V_0 is the volume of the equilibrium and E_0 is the energy of the ground state that corresponds to that volume. The minimum of the curve Etot (V) provides the constant of the equilibrium lattice.

B_0: the compressibility modulus is determined by the following equation:

$$B0 = \left(V\frac{\partial^2 E}{\partial V^2}\right). \quad (2)$$

$B0$: the derivative of the compressibility module:

$$B'0 = \frac{\partial B}{\partial P}. \quad (3)$$

Table 3 lists the results obtained for the structural parameters, together with the available experimental [13] and theoretical results [14], [18], [7], and [23]. Table 3 makes it evident that our results match well with those derived from previous experimental and ab-initio computations. According to Table 3's data, LDA understates the lattice parameter, a, for the B1 structure by roughly 0.39% when compared to the experimental value of 7.067 [13]. However, Table 3 shows that the first derivative of the bulk modulus is underestimated in comparison to the experimental data, and the computed bulk modulus is inflated in LDA, accessible experimental results. In actuality, the bulk modulus and its first derivative values are more susceptible to variations in the parameters employed in ab initio computations.

Table 3. Calculated structural parameters: bulk modulus B_0 and its first derivatives B'_0, equilibrium lattice constants a, and structural parameter c/a for several phases examined for KI

Parameters			NaCl (B1)	CsCl (B2)	ZnS (B3)	WZ (B4)	NiAs (B8_1)	HCP (A3)
KI								
V_0(Å^3)	This Work		87.21	77.933	117.95	116.25	85.13	92.41
	Other work	Theo						
		Exp						
a_0 (Å)	This Work		7.039	4.271	7.784	5.916	4.853	4.027
	Other work	Theo	7.03[c], 7.213[d], 7.094[e]					
		Exp	7.067[a]					
B_0 (GPa)	This Work		15.299	18.535	9.856	8.826	17.35	10.885
	Other work	Theo	11.6[a], 13.8[c]					
		Exp						
B'_0	This Work		3.795	4.226	3.807	4.028	3.335	4.101
	Other work	Theo						
		Exp						
c/a	This Work						1.719	1.633
E_{min}(Ryd)			-15427.90	-15427.886	-15427.88	-15427.8		-15427.3

a-Ref [13], c-Ref [14], d-Ref [18], e-Ref [23], g-Ref [7],

Five other phases are examined in order to examine how atom positions affect the structural characteristics of KI: CsCl (B2), ZnS (B3), WZ (B4), NiAs (B8_1), and HCP (A3). Our results for the B2, B3, B4, B8_1, and A3 phases are predictions and could be used as a guide for future research because, as far as we are aware, no additional ab-initio calculations or experimental data regarding the structural parameters for KI in these phases are available in the literature.

3.2. Phase transition pressure

A change in the lattice structure, or phase transformation, results in a change in the properties. According to experiments, exposing a material to high pressures might result in a noticeable change in its characteristics that indicates modifications to the structures [5, 18, 12, 34]. For instance, numerous tests have demonstrated that the lattice structure changes from RS to CsCl when high pressure is applied to KI.

Using the enthalpy H, which contains the following formula, is a more straightforward and precise way to determine the transition pressure [4, 30].

$$H = E + P.V, \tag{4}$$

At the transformation point, the enthalpy of two structures will be the same. Equation (4) can be used to demonstrate this in the following way:

$$P_t = -\frac{dE}{dV}. \tag{5}$$

$$P_t.dV = -dE. \tag{6}$$

By integrating both sides:

$$Pt\,(V2 - V1) = -(E2 - E1)\,. \tag{7}$$

Rearranging the variables:

$$E1 + Pt\,V1 = E2 + Pt\,V2\,. \tag{8}$$

Using equation (5):

$$H1 = H2. \tag{9}$$

Since both coordinates (enthalpy and pressure) are the same during the phase transformation, a graph of enthalpy vs. pressure for two structures that undergo transition will, in practice, have a crossing point. The transition pressure is the pressure present at this moment. In our earlier study, this approach produced very positive results [35-38, 84, 81, 80, 79]. Fig. 3 displays the enthalpy versus pressure plots that were utilized to determine the transition pressures. Table 4 lists the transition pressure values along with some of the available computed and experimental results. The Pt levels found in this study agree with those found in the previous studies listed in Table 4.

Table 4. Calculated values of the transition pressure Pt and transition volumes for KI using the GGA approximation

Phases	Volume		Transition pressure (GPa)		
	V (Å)^3	Reduct (%)	Presentwork	Other works	
				Theo	Exp
B1→B2	V_{B1} 87.217	10.64	1.633	2[a]	1.73[b] 1.9[c]
	V_{B2} 77.933				

a-Ref. [7], b-Ref. [17], c-Ref. [5]

One transition is predicted by Fig. 3 at the curves' junction sites (equal enthalpies). At roughly 01.633 GPa, the B1 structure gives way to the B2 structure above the crossover from B1 to B2. Our estimated pressure of 1.633 GPa for the B1→B2 transition is quite consistent with the experimental values of Barsch et al. [17] and Assaumi [17], which differ by 18.35%, 5.60 %, and 14.05 %, respectively, and with the earlier theoretical values of 2 GPa found by Ramola *et al.* [7].

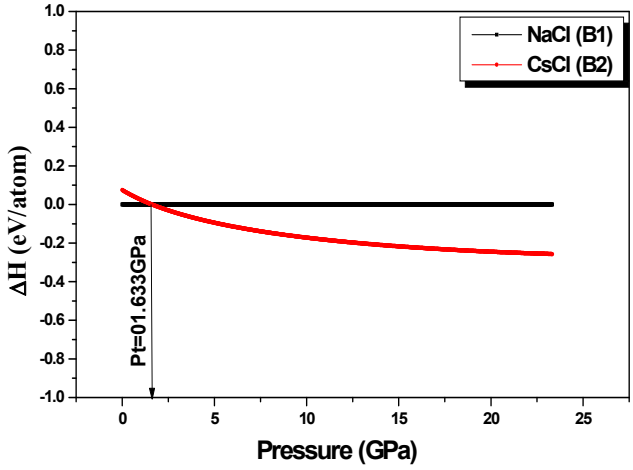

Figure 3. Variation of ΔH (eV/atom) versus Pt (GPa) for CsCl-B2. The reference Gibbs free energy in set for the rocksalt phase NaCl-B1

3.3. Electronic properties

3.2.1. Bande structure

The energy is computed along high symmetry lines, and the band structure (BS) was obtained with the LDA approximation. The optimized lattice constants were used in the calculations. Figure 4 displays the BS graphs for KI in each of the structures that were studied.

The BS graphs show the band gap between the valence and conduction bands. Together with the findings of earlier research on the RS structure, Table 5 lists the values of eg, which is computed as the difference between MVB and MCC. With the other known experimental and theoretical findings, the energy band gap value is underestimated by the LDA approximation. Direct energy band gaps along the Γ symmetry point are observed for the following structures: RS, ZB, NiAs, HCP, and WZ, with values listed in Table (5). In contrast, the CsCl structure exhibits an indirect band gap between the high symmetry points of M and Γ.

In every structure examined in this work (RS, CsCl, ZB, HCP, NiAs, and WZ) the energy band gap values show that KI is a semiconductor.

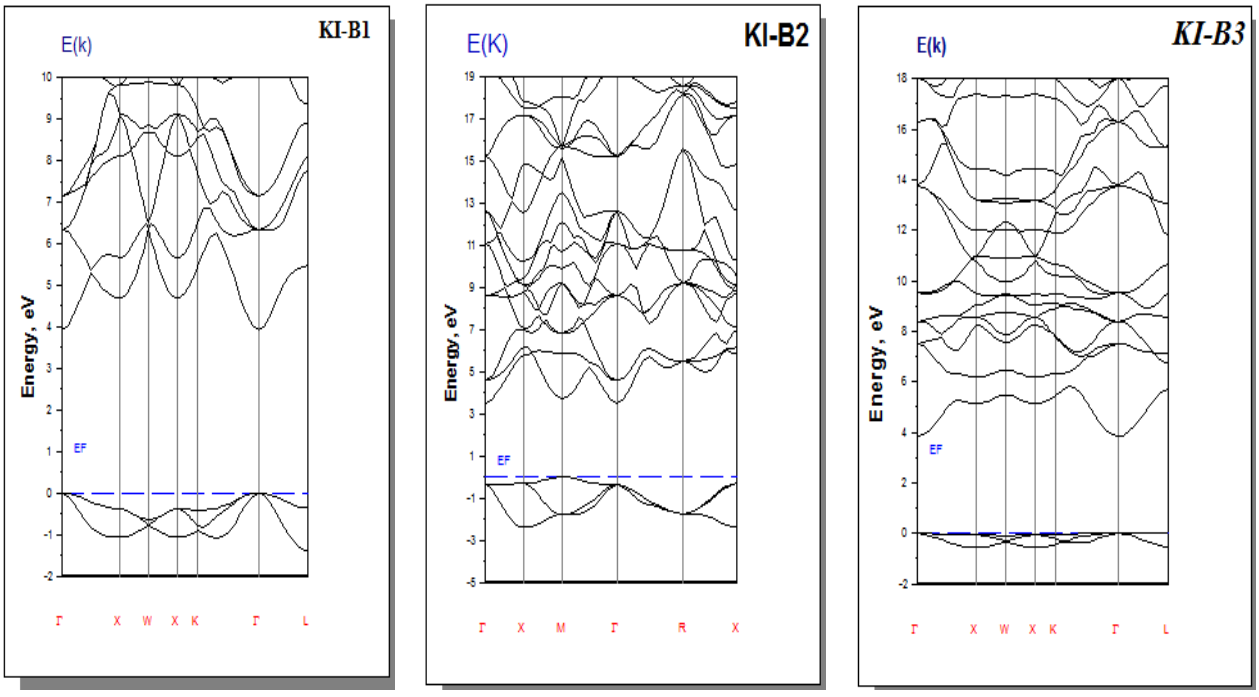

Figure 4. Band structure of KI, in different structures studied

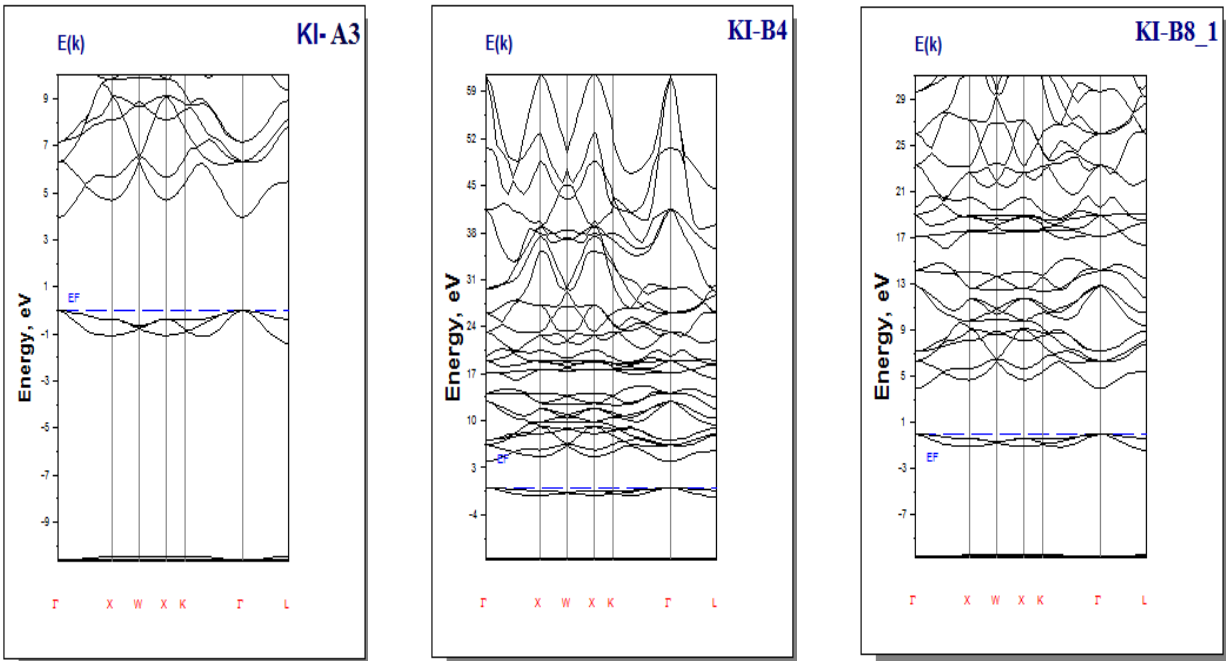

Figure 4. Band structure of KI, in different structures studied
(continued)

Table 5. The gap calculated for KI in different structures studied.

	Phase	Nature of gap	Present work	Type	Other works
KI	**B1**	Γ→Γ	3.936	direct	5.984[b], 6.2[c], 4.26[d], 5.951[e]$_{mBJ}$ 6.34[a]$_{exp}$
	B2	M→Γ	3.512	Indirect	
	B3	Γ→Γ	3.836	direct	
	B4	Γ→Γ		direct	
	B8_1	Γ→Γ		direct	
	A3	Γ→Γ		direct	

a-Ref. [21], b-Ref. [7], c-Ref. [62], d-Ref. [22], e-Ref. [23]

3.2.2. Density of state

As a function of energy, the DOS displays the number of states that electrons can occupy. Figure 5 displays the DOS graphs for KI.

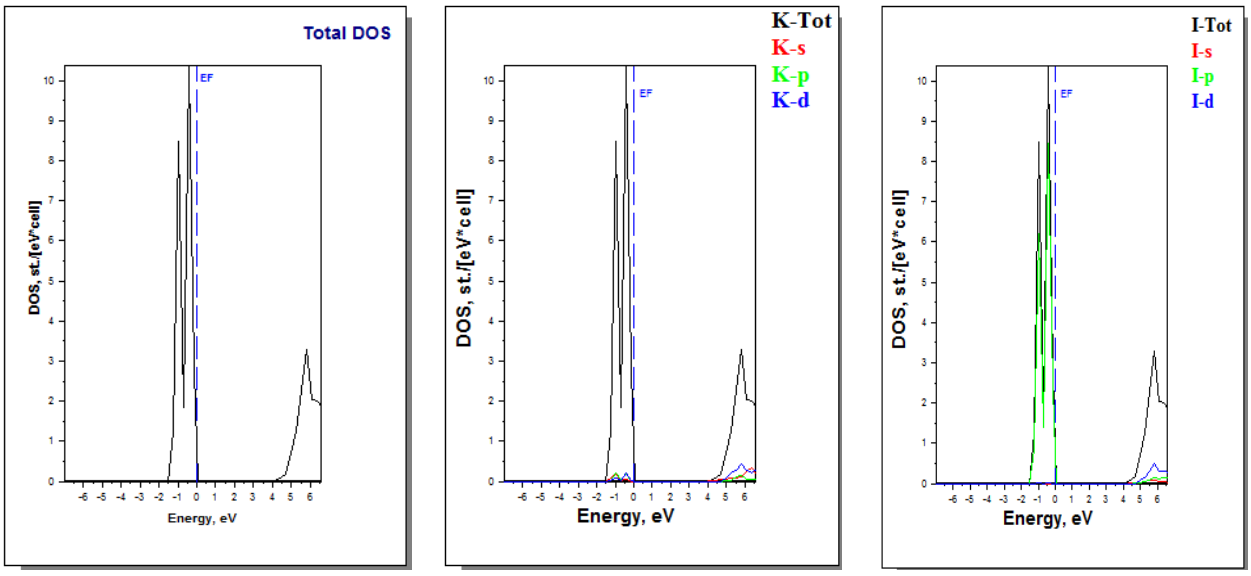

Figure 5. Density of states (DOS) of KI in the different structures studied

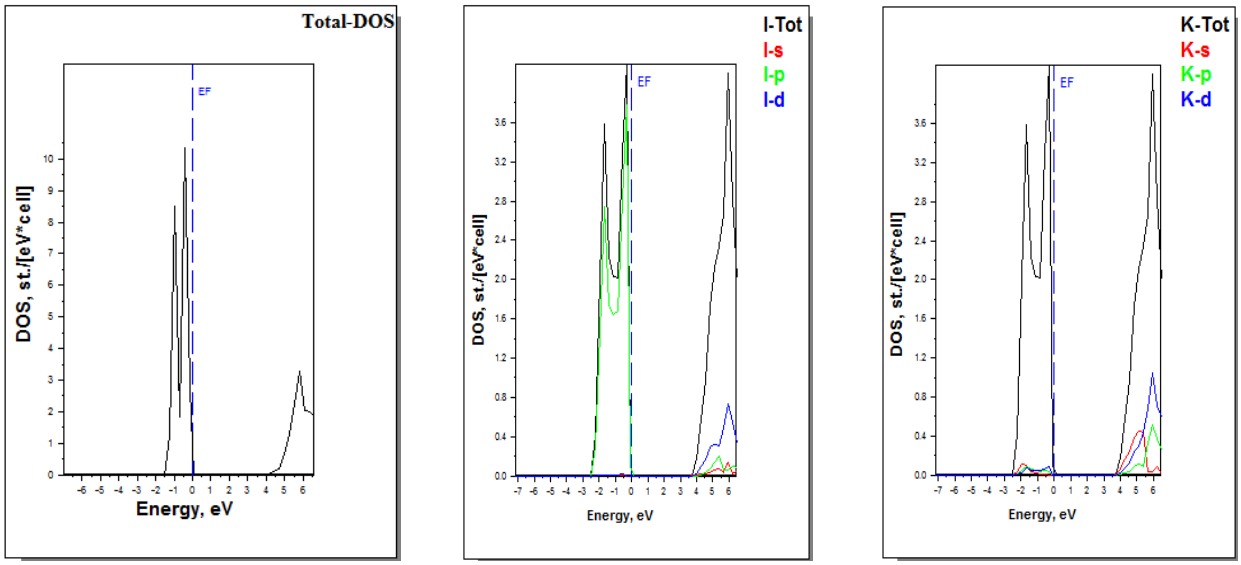

Figure 5. Density of states (DOS) of KI in the different structures studied
(continued)

Since peaks B3, B4, B8_1, and A3 are very identical to peak B1, we did not include them. The Fermi energy (EF) is shown by the dotted line in the DOS graphics. There is only one peak for the energies below the Fermi energy in the structures RS, CsCl, ZB, A3, and NiAs. The p-state in the iodide contributes the most to the DOS, while the p-state in the potassium contributes only a little. In contrast, three peaks are visible in the WZ structure: the first peak is contributed by the potassium's s-state, the second peak combines the contributions of the potassium's p-state and the iodide's s-state, and the third peak is created by the iodide's p-state with a minor contribution from the potassium's p-state.

3.4. Elastic properties

Knowing a material's elastic properties, such as its elastic constants and moduli, allows one to predict how the material will react to external stress. Because of the cubic structures' symmetry, only three elastic constants «C_{11}, C_{12}, and C_{33}» are needed [39], while five elastic coefficients «C_{11}, C_{12}, C_{13}, C_{33}, and C_{55}» were needed for the hexagonal systems [40]. One crucial instrument for assessing a material's stability is its elastic constants. The generalized requirements of stability must be met for a material to be deemed mechanically stable, and they are [41].

$$C_{11} > 0, C_{11} - C_{12} > 0, C_{44} > 0 \; and \; C_{11} + 2C_{12} > 0, \tag{9}$$

for the cubic structures. Additional criteria are required for the hexagonal structures as follows [41]:

$$C_{11} > |C_{12}| \text{ and } C_{55} > 0, \tag{10}$$

where: $C_{44} = C_{55}$ for the hexagonal structures.

When anticipating a material's mechanical characteristics, including its stiffness, hardness, brittleness, and ductility, elastic moduli are crucial. The bulk modulus (B), shear modulus (S), Young's modulus (Y), compressibility (β), anisotropic factor (A), Poisson's ratio (ü), and so on are examples of these elastic moduli.

The elastic properties KI in RS, CsCl, ZB, NiAs and WZ structures at ambient pressure were investigated in this work using the optimized lattice constants. This was accomplished by calculating the stress produced by a tiny strain applied to the optimized unit cell, which in turn led to the computation of the elastic constants. Numerous models have been proposed to determine the elastic moduli in terms of the elastic constants; the most widely used models are the Voigt, [42], Reuss, [43], and Hill [44] models. The Hill model is taken into consideration in this work. The Hill model's bulk modulus is determined by averaging the Voigt and Reuss models' bulk moduli, as follows:

$$B_H = \frac{B_V + B_R}{2}, \tag{11}$$

where $B_H = B_V = B_R = \frac{1}{3}(C_{11} + 2C_{12})$ for the cubic structures[45]. While for the hexagonal structures, the formulas are as follows [45-48]:

$$B_V^{Hex} = \frac{1}{9}(2C_{11} + C_{33} + 2C_{12} + 4C_{13}), \tag{12}$$

$$B_R^{Hex} = \frac{(C_{11}+C_{12})C_{33} - 2C_{13}^2}{C_{11}+C_{12}+2C_{33}-4C_{13}}, \tag{13}$$

$$B_H^{Hex} = \frac{B_V + B_R}{2}. \tag{14}$$

The shear modulus is also calculated using the following formulas [67, 68, 71, 72]

$$S_V^{Cubic} = \frac{C_{11}-C_{12}+3C_{44}}{5}, \tag{15}$$

$$S_R^{Cubic} = \frac{5(C_{11}-C_{12})C_{44}}{3(C_{11}-C_{12})+4C_{44}}, \tag{16}$$

$$S_H^{Cubic} = \frac{S_V^{Cubic}+S_R^{Cubic}}{2}, \tag{17}$$

$$S_V^{Hex} = \frac{1}{30}[7C_{11} - 5C_{12} + 12C_{44} + 2C_{33} - 4C_{13}], \tag{18}$$

$$S_R^{Hex} = \frac{5}{2}\left[\frac{((C_{11}+C_{12})C_{33}-2C_{12}^2)C_{44}C_{66}}{3B_V^{Hex}C_{44}C_{66}+\left((C_{11}+C_{12})C_{33}-2C_{12}^2\right)(C_{44}+C_{66})}\right], \tag{19}$$

with C_{66} being given as [48-50].

$$C_{66} = \frac{1}{2}(C_{11} - C_{12}), \tag{20}$$

$$S_H^{Hex} = \frac{S_V^{Hex}+S_R^{Hex}}{2}. \tag{21}$$

The following formulas [51, 52] are used to compute the Young's modulus (Y) and Poisson's ratio using the Hill model results of the bulk and shear moduli.

$$Y = \frac{9SB}{S+3B}, \tag{22}$$

$$\upsilon = \frac{3B-2S}{2(3B+S)}. \tag{23}$$

The anisotropy factor and the material's hardness were among the other variables that were computed. The relations [53,54] were used to compute the anisotropic factor.

$$A_{Cubic} = \frac{2C_{44}}{C_{11}-C_{12}}, \tag{24}$$

$$A_{Hex} = \frac{4C_{44}}{C_{11}+C_{33}-2C_{13}}. \tag{25}$$

Chen's Vickers hardness formula, which is as follows [55], was applied to determine the hardness.

$$H_\upsilon = 2(\frac{S^3}{B^2})^{0.585} - 3. \tag{26}$$

Moreover, Cauchy pressure (Cs) was calculated using the forms as [56]:

$$C_S^{Cubic} = C_{12} - C_{44}, \tag{27}$$

$$C_S^{Hex} = C_{12} - C_{55}. \tag{28}$$

The Born's conditions are satisfied by the elastic constants for KI in the RS, CsCl, Wz, HCP, and ZB structures displayed in Table 6 [57]. Using Murnaghan's equation of state [30], the values for the bulk modulus are in excellent agreement with the findings shown in tables 3. The structures RS, CsCl, ZB, and WZ have low bulk modulus values, which suggest that they have poor resistance to breaking under pressure. On the other hand, because of its largest bulk modulus value, CsCl is thought to be the hardest structure for KI and the least compressible (β =1/B).

Out of all the structures, the ZB structure has the maximum compressibility and the lowest bulk modulus.

Table 6. The elastic constants, the bulk modulus calculated by Hill's approximation for KI in RS, CsCl and ZB and Wz structures in (GPa)

Phase		C_{11}	C_{12}	C_{44}	B	C_{13}	C_{33}	C_{55}
NaCl (B1)	***This Work***	24.1738	3.890	3.8400	10.651			
	Exp Reslt	27.1[a] 33.2[b]	4.5[a] 5.78[b]	3.64[a] 6.2[b]				
	Othr Theor	31.7[c]	3.2[c]	4.2[c]				
CsCl (B2)	***This Work***	33.9234	3.195	2.3456	13.437			
ZnS (B3)	***This Work***	7.5379	6.916	5.0597	7.123			
WZ (B4)	***This Work***	14.7989	5.610		9.543	7.9129	13.485	3.222

a-Ref. [24], b-Ref. [25], c-Ref. [19].

Table 7 shows the factors and elastic moduli. If the anisotropic component A=1, the material is said to be totally isotropic; any departure indicates the degree of anisotropy. Since none of the structures « RS, CsCl, and ZB » have an isotropy of one, they all exhibit anisotropic behavior. Conversely, the WZ structure exhibits isotropic behavior with an isotropy of nearly 1.

Table 7. For KI compound in RS, CsCl, ZB, and WZ structures, the computed Hill's Shear modulus (SH), Young's modulus (YH) in (GPa), Poisson's ratio (υH), the anisotropic ratio (A), the B/S ratio, the Cauchy pressure (PC) in (GPa), the compressibility (β) in (1/GPa), and the Hardness (H)

Symbol	NaCl (B1)	CsCl (B2)	ZnS (B3)	WZ (B4)
S_H	5.735	5.55	1.935	3.565
Y_H	14.586	14.635	5.322	9.51
υ_H	0.271	0.318	0.375	0.333
A	0.3786	0.1527	16.2875	1.0358
B_H/S_H	1.8572	2.4211	3.6811	2.6768
C_S	0.0504	0.8496	1.8569	2.3838
β_H	0.0938	0.7442	0.1404	0.1048
H_υ	-0.3071	-0.0629	-2.35947	-1.6705

The (B/S) ratio can be used to assess a material's brittleness or ductility. Every structure in Table 7 has B/S ratios greater than 1.75, indicating that the KI in those structures is ductile. In contrast, the RS has the highest shear modulus, which is extremely near to that of the CsCl structure. A material's stiffness can be studied using Young's modulus (Y); the greater the value of Y, the stiffer the material. With the largest value of Y, the CsCl structure of KI appears to be the stiffest structure. This is supported by the fact that the CsCl structure has the highest hardness (H). In contrast, the ZB structure has the lowest Y and H, making it the least stiff. The inferences drawn from the bulk modulus values are supported by these findings.

All of the structures in Table 7 exhibit positive Cauchy's pressure (Cs) values, indicating that ionic bonding is the predominant bonding type. Although ionic bonds remain the predominant form of bonding, it is reasonable to state that the RS structure has the "highest covalent bonding" of all because its Cs has the lowest value, which is quite near to zero. Since all of the υ values are greater than 0.25, which indicates ionic bonding inside the material, this is consistent with the Poisson's ratio results.

5. CONCLUSION

Potassium iodide was investigated using the FP-LMTO technique within the density functional theory (DFT) and the LDA Approximation in a number of distinct structures, including RS, CsCl, ZB, NiAs, HCP, and WZ. The adjusted lattice parameters and bulk modulus matched previous theoretical and experimental results. Using the LDA approximation, band gaps were determined and compared to the findings of existing theoretical and experimental research. The resulting values are lower than the reference values, which should be noted. It is well known that LDA lowers band gaps. The improved lattice constants were also used to analyze the elastic properties. The elastic constants for the RS, CsCl, ZB and WZ structures satisfied Born's stability requirements. The CsCl structure had the highest bulk modulus when compared to other structures, suggesting that it was more resistant to breaking. In contrast, the ZB structure exhibited the lowest bulk modulus. Poisson's ratio values varied from 0.271 to 0.375, despite the fact that all structures had positive Cauchy pressure values, which suggested ionic bonding inside the lattice. It was found that the ZB structure had the lowest hardness and the RS structure the highest. The rigidity of the materials was assessed using Young's modulus, where the ZB structure had the lowest value and the RS structure the highest. For all stable structures, the anisotropic component (A) was found to be anisotropic, with values that were far from unity.

ORCID

Hamza Rekab Djabri, https://orcid.org/0000-0002-2458-1335; **Ahmed Azzouz Rached,** https://orcid.org/0000-0003-4852-1000
Ammar Benamrani, https://orcid.org/0000-0002-6886-656X; **Djamel Belfennache,** https://orcid.org/0000-0002-4908-6058

REFERENCE

[1] B.P. Mamula, B. Kuzmanović, M.M. Ilić, N. Ivanović, and N. Novaković, Physica B: Condensed Matter, **545**(36), 146 (2018). https://doi.org/10.1016/j.physb.2018.06.008
[2] R.G. Bessent, and A.W. Runciman, Br. J. Appl. Phys. **17(8)**, 991 (1966). https://doi.org/10.1088/0508-3443/17/8/302
[3] L.S. Combes, S.S. Ballard, and K.A. McCarthy, JOSA, **41(4)**, 215 (1951). https://doi.org/10.1364/JOSA.41.000215
[4] J.T. Lewis, A. Lehoczky, and C.V. Briscoe, Phys. Rev. **161(3)**, 877 (1967) https://doi.org/10.1103/PhysRev.161.877
[5] K. Asaumi, and Mori, T. Phys. Rev. B, **28**(6), 3529 (1983). https://doi.org/10.1103/PhysRevB.28.3529
[6] K.J. Teegarden, Phys. Rev. **105**(4), 1222 (1957). https://doi.org/10.1103/PhysRev.105.1222
[7] Y. Ramola, C.N. Louis, and A. Amalraj, Chem. Mater. Eng. **5**(3), 65 (2017). https://doi.org/10.13189/cme.2017.050302
[8] Y. Ramola, J. Merlinebetsy, C.N. Louis, and A. Amalraj, Chemical and Materials Engineering, **7**(2), 9 (2019). https://doi.org/10.13189/cme.2019.070201
[9] The COSINE-100 Collaboration, **564**, 83 (2018). https://doi.org/10.1038/s41586-018-0739-1
[10] C. Yam, C. Ma, X. Wang, and G. Chen, Appl. Phys. Lett. **85**(19), 4484 (2004). https://doi.org/10.1063/1.1819510

[11] I. Ohlídal, and D. Franta, Handbook of Optical Constants of Solids, **3**, 857 (1997). https://doi.org/10.1016/B978-012544415-6.50136-9
[12] R.B. Jacobs, Phys. Rev. **54**(6), 468 (1938). https://doi.org/10.1103/PhysRev.54.468
[13] S.T. Weir, J. Akella, C. Aracne-Ruddle, Y.K. Vohra, and S.A. Catledge, Appl. Phys. Lett. **77**(21), 3400 (2000). https://doi.org/10.1063/1.1326838
[14] P. Cortona, Phys. Rev. B, **46**, 2008 (1992). https://doi.org/10.1103/PhysRevB.46.2008
[15] Z.P. Chang, and G.R. Barsch, J. Phys. Chem. Solids, **32**(1), 27 (1971). https://doi.org/10.1016/S0022-3697(71)80005-7
[16] M. Ghafelehbashi, D.P. Dandekar, and A.L. Ruoff, J. Appl. Phys. **41**(2), 652 (1970). https://doi.org/10.1063/1.1658728
[17] G.R. Barsch, and H.E. Shull, Physica status solidi (b), **43**(2), 637 (1971). https://doi.org/10.1002/pssb.2220430224
[18] A. Asenbaum, O. Blaschko, and H.D. Hochheimer, Phys. Rev. B, **34**(3), 1968 (1986). https://doi.org/10.1103/PhysRevB.34.1968
[19] A.K. Sarkar, and S. Sengupta, Physica status solidi (b), **36**(1), 359 (1969). https://doi.org/10.1002/pssb.19690360137
[20] K. Teegarden, and G. Baldini, Phys. Rev. **155**(3), 896 (1967). https://doi.org/10.1103/PhysRev.155.896
[21] J.J. Hopfield, and J.M. Worlock, Phys. Rev. **137**, A1455 (1965). https://doi.org/10.1103/PhysRev.137.A1455
[22] J. Li, C.G. Duan, Z.Q. Gu, and D.S. Wang, Phys. Rev. B, **57**(4), 2222 (1998). https://doi.org/10.1103/PhysRevB.57.2222
[23] M. Bashi, H.R, Aliabad, A.A. Mowlavi, I. Ahmad, Solid State Nucl. Magn. Reson. **82**, 10 (2017). https://doi.org/10.1016/j.ssnmr.2016.12.009
[24] M.H. Norwood, and C.V Briscoe, Physical Review, **112**(1), 45 (1958). https://doi.org/10.1103/PhysRev.112.45
[25] P.W. Bridgman, Proc. Am. Acad. Arts Sci. **64**, 305 (1929). http://nobelprize.org/nobel_prizes/physics/laureates/1946/bridgman-bio.html
[26] C. Gahn, and A. Mersmann, Chem. Eng. Sci. **54**(9), 1273 (1999). https://doi.org/10.1016/S0009-2509(98)00450-3
[27] Y. Benkrima, D. Belfennache, R. Yekhlef, and A.M. Ghaleb, Chalcogenide Lett. **20,** 609 (2023). https://doi.org/10.15251/CL.2023.208.609
[28] Y. Achour, Y. Benkrima, I. Lefkaier, and D. Belfennache, J. Nano- Electron. Phys. **15**(1), 01018 (2023) https://doi.org/10.21272/jnep.15(1).01018
[29] Y. Benkrima, D. Belfennache, R. Yekhlef, M.E. Soudani, A. Souiga, and Y. Achour, East Eur. J. Phys. (2), 150 (2023). DOI:10.26565/2312-4334-2023-2-14
[30] H.R. Djabri, R. Khatir, S. Louhibi-Fasla, I. Messaoudi, and H. Achour, Comput. Condens. Matter, **10**, 15 (2017). https://doi.org/10.1016/j.cocom.2016.04.003
[31] Y. Benkrima, A. Achouri, D. Belfennache, R. Yekhlef, and N. Hocine, East Eur. J. Phys. (2), 215 (2023). DOI:10.26565/2312-4334-2023-2-23
[32] Y. Benkrima, S. Benhamida, and D. Belfennache, Dig. J. Nanomater. Bios. **18**(1), 11 (2023) https://doi.org/10.15251/DJNB.2023.181.11
[33] Y. Benkrima, M.E. Soudani, D. Belfennache, H. Bouguettaia, and A. Souigat, J. Ovonic. Res. **18**(6), 797 (2022). https://doi.org/10.15251/JOR.2022.186.797
[34] H.G. Drickamer, R.W. Lynch, R.L. Clendenen, and E.A. Perez-Albueene, Solid State Phys. **19**, 135 (1967). https://doi.org/10.1016/S0081-1947(08)60529-9
[35] N. Beloufa, Y. Cherchab, S. Louhibi-Fasla, S. Daoud, H. Rekab-Djabri, and A. Chahed, Comput. Condens. Matter. **30**, e00642 (2022). https://doi.org/10.1016/j.cocom.2022.e00642
[36] N. Rahman, M. Husain, W. Ullah, A. Azzouz-Rached, Y.M. Alawaideh, H. Albalawi, Z. Bayhan, *et al*., Inorg. Chem. Commun. **166**, 112625 (2024). https://doi.org/10.1016/j.inoche.2024.112625
[37] S. Daoud, P.K. Saini, and H. Rekab-Djabri, J. Nano- Electron. Phys. **12**(6), 06008 (2020). https://doi.org/10.21272/jnep.12(6).06008
[38] R. Yagoub, H.R. Djabri, S. Daoud, N. Beloufa, M. Belarbi, A. Haichour, C. Zegadi, and S.L. Fasla, Ukr. J. Phys. **66**, 699 (2021). DOI: 10.15407/ujpe66.8.699
[39] J. Yan, J. Zhao, J. Sheng, B. Wang, and J. Zhao, Mater. Today Commun. **41,** 110966 (2024). https://doi.org/10.1016/j.mtcomm.2024.110966
[40] K. Burke, Friends, *The ABC of DFT*, (Department of Chemistry, University of California, Irvine, CA 2007).
[41] J.P. Perdew, Phys. Rev. B, **33**(12), 8822 (1986). https://doi.org/10.1103/PhysRevB.33.8822
[42] J.P. Perdew, K. Burke, and M. Ernzerhof, Phys. Rev. Lett. **77**(18), 3865 (1996). https://doi.org/10.1103/PhysRevLett.77.3865
[43] A.D. Becke, and E.R. Johnson, J. Chem. Phys. **124**(22), 221101 (2006). https://doi.org/10.1063/1.2213970
[44] R. Hill, Proc. Phys. Soc. A, **65**, 349 (1952). https://doi.org/10.1088/0370-1298/65/5/307
[45] J.P. Perdew, J. Tao, V.N. Staroverov, and G.E. Scuseria, J. Chem. Phys. **120**(15), 6898 (2004). https://doi.org/10.1063/1.1665298
[46] A.D. Becke, and E.R. Johnson, J. Chem. Phys. **124**(22), 221101 (2006). https://doi.org/10.1063/1.2213970
[47] A.D. Becke, and M.R. Roussel, Phys. Rev. A, **39(8)**, 3761 (1989). https://doi.org/10.1103/PhysRevA.39.3761
[48] F. Tran, and P. Blaha, Phys. Rev. Lett. **102**(22), 226401 (2009). https://doi.org/10.1103/PhysRevLett.102.226401
[49] Y. Guermit, K. Hocine, M. Drief, T. Lantri, H. Rekab-Djabri, A. Maizia, and N.E. Benkhettou, Opt. Quant. Electron. **56**(4), 537 (2024). https://doi.org/10.1007/s11082-023-06056-1
[50] F. Benguesmia, A. Benamrani, L. Boutahar, H. Rekab-Djabri, and S. Daoud, J. Phys. Chem. Res. **1**(2), 25 (2022). https://doi.org/10.58452/jpcr.v1i2.24
[51] J. Jiang, J. Chem. Phys. **138**(13), 134115 (2013). https://doi.org/10.1063/1.4798706
[52] O.K. Andersen, Phys. Rev. B, **12**(8), 3060 (1975). https://doi.org/10.1103/PhysRevB.12.3060
[53] R. Jaradat, M. Abu-Jafar, I. Abdelraziq, S.B. Omran, D. Dahliah, and R. Khenata, Mater. Chem. Phys. **208**, 132 (2018). https://doi.org/10.1016/j.matchemphys.2018.01.037
[54] P. Blaha, K. Schwarz, P. Sorantin, and S.B. Trickey, Comput. Phys. Commun. **59**(2), 399 (1990). https://doi.org/10.1016/0010-4655(90)90187-6
[55] H. Ibach, and H. Lueth, Solid-state physics. An introduction to principles of materials science, (Springer, Berlin, 2009). https://doi.org/10.1007/978-3-540-93804-04

[56] S.H. Simon, *Problems for Solid State Physics*, (3rd Year Course 6) Hilary Term, (Oxford University, 2011).
[57] M. Born, K. Huang, and M. Lax, Journal of Physics, **23**(7), 474 (1955). https://doi.org/10.1119/1.1934059

СТРУКТУРНІ, ЕЛЕКТРОННІ ТА ПРУЖНІ ВЛАСТИВОСТІ ЙОДИДУ КАЛІЮ ПІД ТИСКОМ: ДОСЛІДЖЕННЯ AB-INITIO

Хамза Рекаб-Джабрі[a,b], С. Зайоу[c,d], Ахмед Аззуз-Рашед[e], Аммар Бенамрані[f], Салах Дауд[g], Д. Белфеннаше[h], Р. Єхлеф[h], Набіль Белуфа[i]

[a]*Лабораторія мікро- та нанофізики (LaMiN), Національна політехнічна школа Орана, ENPO-MA, BP 1523 Ель-М'Науер 31000, Оран, Алжир*
[b]*Факультет природничих наук та наук про Землю, Університет АМО, Буйра 10.000, Алжир*
[c]*Лабораторія досліджень поверхонь та меж розділу твердих матеріалів (LESIMS), Університет Сетіф 1, 19000 Сетіф, Алжир*
[d]*Факультет природничих наук та наук про життя, Сетіф-1 Університет, 19000 Сетіф, Алжир*
[e]*Факультет наук, Університет Саада Дахлеба в Бліді 1, вул. Соумаа, В. Р. 270, Бліда, Алжир*
[f]*Лабораторія фізики матеріалів, радіації та наноструктур (LPMRN), Факультет наук і технологій, Університет Мохамеда Ель Бачіра Ель Ібрагімі-BBA, 34000, Бордж Бу Арреріджс, Алжир*
[g]*Лабораторія матеріалів та електронних систем, Факультет наук і технологій, Університет Мохамеда Ель Бачіра Ель Ібрагімі, BBA, 34000 Бордж Бу Арреріджс, Алжир*
[h]*Науково-дослідний центр промислових технологій CRTI, P.O. A/c 64, Черага, 16014 Алжир, Алжир*
[i]*Гідрометеорологічний інститут формування та досліджень IHFR, Оран, Алжир*

У цій роботі було використано нещодавню версію методу повного потенціалу лінійних мафін-тинових орбіталей (FP-LMTO) з використанням наближення локальної густини (LDA) в рамках теорії функціоналу густини (DFT). Цей підхід було застосовано для вивчення структурної, електронної та пружної поведінки сполуки йодиду калію (KI) під тиском. Розраховані структурні параметри демонструють сильну відповідність з наявними теоретичними та експериментальними даними. Фаза RS була визначена як найстабільніша структура для матеріалу KI. Фазовий перехід від фази типу NaCl (B1) до фази типу CsCl (B2) відбувається при тиску 1,633 ГПа, що цілком узгоджується з експериментальними значеннями. Крім того, зонна структура KI виявила широкозонну напівпровідникову поведінку у всіх досліджених фазах. Отримані значення модуля об'ємної пружності були відносно низькими, що свідчить про слабку стійкість до руйнування. Було визначено константи пружності для KI в структурах RS, CsCl, ZnS, HCP та WZ, які відповідають умовам стійкості Борна. Ми вважаємо, що в літературі немає значень констант пружності для KI у фазах CsCl, ZnS та WZ. Усі аналізовані структури демонстрували пластичні характеристики та особливості іонних зв'язків. Крім того, анізотропні властивості спостерігалися у всіх фазах. Жорсткість сполуки оцінювали за допомогою коефіцієнта Пуассона та тиску Коші. Результати показали, що фаза CsCl є найжорсткішою серед досліджуваних конфігурацій.

Ключові слова: *йодид калію (KI); FP-LMTO; електронні властивості; еластичні властивості; фазовий перехід*